Manipulating L-type calcium channels in cardiomyocytes using split-intein protein transsplicing

Prakash Subramanyam, Donald D. Chang, Kun Fang, Wenjun Xie, Andrew R. Marks, and Henry M. Colecraft[1]

Department of Physiology and Cellular Biophysics, Columbia University, New York, NY 10032

Edited by Kurt G. Beam, University of Colorado at Denver, Aurora, CO, and approved August 6, 2013 (received for review April 30, 2013)

Manipulating expression of large genes (>6 kb) in adult cardiomyocytes is challenging because these cells are only efficiently transduced by viral vectors with a 4–7 kb packaging capacity. This limitation impedes understanding structure–function mechanisms of important proteins in heart. L-type calcium channels (LTCCs) regulate diverse facets of cardiac physiology including excitation–contraction coupling, excitability, and gene expression. Many important questions about how LTCCs mediate such multidimensional signaling are best resolved by manipulating expression of the 6.6 kb pore-forming α_{1C}-subunit in adult cardiomyocytes. Here, we use split-intein–mediated protein transsplicing to reconstitute LTCC α_{1C}-subunit from two distinct halves, overcoming the difficulty of expressing full-length α_{1C} in cardiomyocytes. Split-intein–tagged α_{1C} fragments encoding dihydropyridine-resistant channels were incorporated into adenovirus and reconstituted in cardiomyocytes. Similar to endogenous LTCCs, recombinant channels targeted to dyads, triggered Ca^{2+} transients, associated with caveolin-3, and supported β-adrenergic regulation of excitation–contraction coupling. This approach lowers a longstanding technical hurdle to manipulating large proteins in cardiomyocytes.

CaV1.2 | ventricular myocytes | gene transfer | protein splicing

Adult ventricular cardiomyocytes have a unique cytoarchitecture and intracellular milieu (including transverse tubules, dyadic junctions, and ryanodine receptors) that is not replicated in many other cell types (1). Consequently, many fundamental questions regarding structure–function mechanisms of cardiac signaling proteins can only be pursued in the context of native cardiomyocytes. Knock-in mouse models are unarguably the gold standard for structure–function studies of signaling proteins in heart. However, the high cost (~$50,000) and length of time (up to 2 y) required to generate a single knock-in mouse makes it impractical to routinely use this model system for investigative studies of structure–function mechanisms in heart cells. Directly manipulating expression of target proteins in adult cardiomyocytes is an important tool for structure–function studies in heart (2). However, this approach is challenging because (*i*) adult cardiomyocytes are refractory to transfection using conventional methods and (*ii*) they can only be maintained in culture for short periods (3–4 d) before they dedifferentiate (2). Fortunately, adult cardiomyocytes are efficiently transduced by viral vectors. A major technical hurdle is that commonly used viral vectors have a packaging capacity of 4–7 kb (2, 3).

Studies of the cardiac L-type calcium channel (LTCC) illustrate these challenges. In heart, LTCCs mediate excitation–contraction (EC) coupling, control excitability, and regulate gene expression (1, 4). In ventricular myocytes, the majority of LTCCs are targeted to transverse tubules where they are closely apposed to intracellular Ca^{2+} release channels, ryanodine receptors (RyR2), at dyadic junctions (4, 5) (Fig. 1*A*). This spatial arrangement is critical for the high gain of Ca^{2+}-induced Ca^{2+} release (CICR) that underlies cardiac EC coupling (6). A subset of cardiac LTCCs are found located in caveolae (7), and are hypothesized to selectively signal through local effectors to the nucleus (8, 9) (Fig. 1*A*). Cardiac LTCC currents are increased several-fold by protein kinase A (PKA), which is activated via β-adrenergic signaling (10). The molecular mechanisms and determinants underlying LTCC targeting to dyads and caveolae and modulation by PKA are either unknown or ambiguous. Reconstituting LTCCs in heterologous cells to address such questions has proven inadequate because these cells are deficient in essential structural elements such as transverse (t) tubules (Fig. 1*B*), and also lack a permissive environment for PKA modulation (11, 12). Moreover, because resolving these structure–function questions will likely require many different constructs, it is impractical to use knock-in mice for such investigative purposes. Hence, directly manipulating LTCCs in isolated adult ventricular myocytes is critical for addressing these questions. Cardiac LTCCs are multisubunit proteins containing a pore-forming α_{1C} assembled with auxiliary β and $\alpha_2\delta$ subunits, and calmodulin (13) (Fig. 1*C*). The 6.6 kb size of α_{1C} is at the packaging capacity of commonly used viral vectors, making it difficult to generate viral vectors incorporating full-length α_{1C}. This deficiency has been a major roadblock to progress in determining structure–function mechanisms of cardiac LTCCs.

To overcome the obstacle of routinely expressing LTCC α_{1C} and other large proteins in adult cardiomyocytes, we developed an approach that relies on split-intein–mediated protein transsplicing. Inteins are naturally occurring protein-splicing elements found in archaeal, eubacterial, and eukaryotic genes (14). When attached to two different polypeptides (termed "exteins"), trans-acting split inteins can rapidly associate to form an active intein that uses a self-catalytic reaction to splice the two exteins together with a peptide bond while excising itself out of the resulting protein sequence (15, 16). We used the split DnaE intein from the cyanobacterium *Nostoc punctiforme* (17, 18) to reconstitute full-length α_{1C} in situ from two separate halves. The split-intein–tagged α_{1C} fragments readily incorporated into adenovirus and reconstituted dihydropyridine (DHP)-resistant channels in cardiomyocytes. Similar to endogenous LTCCs, intein-spliced α_{1C} subunits targeted to dyads, triggered Ca^{2+} transients, associated with caveolin-3, and supported PKA regulation of EC coupling.

Significance

Manipulating expression of proteins directly in isolated heart cells is an important method to study cardiac biology and disease. However, this approach is challenging for large genes (>6 kb) because these exceed the packaging capacity of commonly used viral vectors used to deliver genes into heart cells. Here, we used a split-intein–mediated protein transsplicing strategy to reconstitute the large pore-forming subunit of L-type calcium channels from two separate fragments in heart cells. This approach provides a general method to express different large proteins in heart cells and will help advance new insights into basic mechanisms underlying cardiac function and disease.

Author contributions: P.S. and H.M.C. designed research; P.S., D.D.C., K.F., and W.X. performed research; A.R.M. contributed new reagents/analytic tools; P.S. and H.M.C. analyzed data; and P.S. and H.M.C. wrote the paper.

The authors declare no conflict of interest.

This article is a PNAS Direct Submission.

[1]To whom correspondence should be addressed. E-mail: hc2405@columbia.edu.

This article contains supporting information online at www.pnas.org/lookup/suppl/doi:10.1073/pnas.1308161110/-/DCSupplemental.

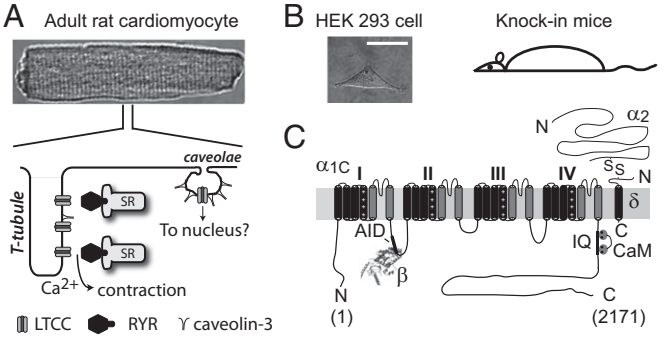

Fig. 1. Model systems for structure–function studies of cardiac LTCCs. (*A*, *Upper*) Adult rat ventricular cardiomyocyte. (*A*, *Bottom*) Differential LTCC targeting to distinct subcellular microdomains in cardiomyocytes. (*B*) Model systems for LTCC structure–function studies. (Scale bar, 20 μm.) (*C*) Topology of LTCC pore-forming α_{1C} and auxiliary proteins (β, α2δ, and calmodulin).

Results

Design and Functional Properties of Split-Intein–Spliced α_{1C} Reconstituted in HEK293 Cells. LTCC α_{1C} subunit is a 2,171-residue protein containing four homologous domains each with six transmembrane segments and cytoplasmic *N* and C termini (19) (Fig. 1*C*). The homologous domains are joined by long intracellular loops. We split α_{1C} cDNA at the II–III loop and cloned the split-intein fragments of *N. punctiforme* DnaE intein into the C and *N* termini of the left ($[I–II]_{N\text{-intein}}$) and right ($_{C\text{-intein}}[III–IV]$) halves, respectively (Fig. 2*A* and Fig. S1). To visualize and distinguish reconstituted channels from endogenous LTCCs, we attached CFP and YFP to the *N* and C termini of $[I–II]_{N\text{-intein}}$ and $_{C\text{-intein}}[III–IV]$, respectively; engineered an extracellular epitope tag (bungarotoxin-binding site, BBS) (20, 21) into domain II S5–S6 loop of $_{CFP}[I–II]_{N\text{-intein}}$; and introduced two mutations (T1066Y/Q1070M) into $_{C\text{-intein}}[III–IV]_{YFP}$ that render LTCCs relatively insensitive to DHP blockers (DHP–) (22, 23) (Fig. 2*A*). When coexpressed in cells, we predicted $_{CFP}[I–II]_{N\text{-intein}}$ and $_{C\text{-intein}}[III–IV]_{YFP}$ would interact to form a spliced α_{1C} intermediate in which the split *N. punctiforme* DnaE inteins associate to form an active intein. The active intein would then use a self-catalyzed reaction to splice the two channel halves together while excising itself out (Fig. 2*A*). Typically, three intein residues—cysteine, phenylalanine, and asparagine—are left behind in the spliced product. Taking advantage of an endogenous asparagine residue at the split site, we designed constructs so that the splicing reaction leaves behind only two foreign residues, cysteine and phenylalanine (Fig. S1).

We first used Western blotting to determine whether coexpression of split-intein–tagged α_{1C} moieties in HEK293 cells resulted in a reconstituted full-length protein as conceptualized in Fig. 2*A*. In cells expressing either $_{CFP}[I–II]_{N\text{-intein}}$ or $_{C\text{-intein}}[III–IV]_{YFP}$ alone, respectively, anti-GFP (which recognizes both CFP and YFP) Western blots revealed bands corresponding to the two half proteins (Fig. 2*B*, lanes 2 and 3). In cells coexpressing $_{CFP}[I–II]_{N\text{-intein}}$ and $_{C\text{-intein}}[III–IV]_{YFP}$, we detected a higher molecular weight band at the expected size of the spliced WT α_{1C} channel product (Fig. 2*B*, lane 4). We similarly detected the spliced DHP-resistant α_{1C} channel when $_{CFP}[I–II]_{N\text{-intein}}$ was coexpressed with $_{C\text{-intein}}[III–IV^{TQ/YM}]_{YFP}$ (Fig. 2*B*, lane 5). The transsplicing reaction was highly efficient, as evidenced by the complete consumption of the moiety with limiting expression ($_{C\text{-intein}}[III–IV]_{YFP}$) in the reaction (Fig. 2*B*, lanes 4 and 5). The high efficiency of the transsplicing reaction is likely aided by the fact that the I–II and III–IV domains of Ca_V channels have a natural affinity for each other and interact when coexpressed (24–26). By titrating the relative amount of $_{CFP}[I–II]_{N\text{-intein}}$ to $_{C\text{-intein}}[III–IV]_{YFP}$ cDNA transfected, it was possible to approach a balanced level of expression where both fragments were essentially used up in the splicing reaction (Fig. 2*C*).

We next determined whether intein-spliced α_{1C} had similar functional properties to full-length (WT) α_{1C} subunit expressed in HEK293 cells. First, WT α_{1C} requires coexpression of $Ca_V\beta$

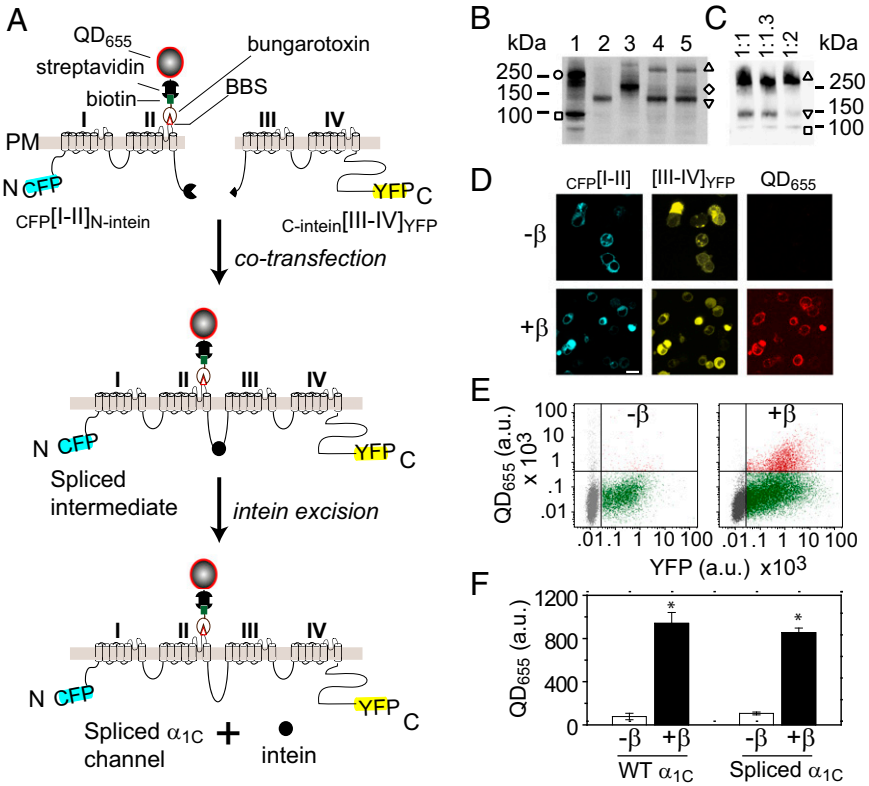

Fig. 2. Reconstituting LTCCs by split-intein–mediated protein transsplicing. (*A*) Strategy for reconstituting full-length α_{1C} using split-intein–mediated protein splicing. The α_{1C} subunit is split into two halves tagged with fluorophores and flanking *N. punctiforme* DnaE split inteins, creating $_{CFP}[I–II]_{N\text{-intein}}$ and $_{C\text{-intein}}[III–IV]_{YFP}$, respectively. A 13-residue BBS tag is introduced to permit selective labeling of surface channels with quantum dot (QD_{655}). (*B* and *C*) Anti-GFP Western blot showing successful reconstitution of covalently linked full-length α_{1C} from intein-flanked α_{1C} moieties in HEK293 cells. Lane 1, full-length α_{1C}[BBS]–YFP (open circle) + β_{2a}-CFP (open square); lane 2, $_{CFP}[I–II]_{N\text{-intein}}$ (inverted triangle); lane 3, $_{C\text{-intein}}[III–IV]_{YFP}$ (open diamond); lane 4, $_{CFP}[I–II]_{N\text{-intein}}$ + $_{C\text{-intein}}[III–IV]_{YFP}$ (open triangle); lane 5, $_{CFP}[I–II]_{N\text{-intein}}$ + $_{C\text{-intein}}[III–IV^{TQ/YM}]_{YFP}$ (open triangle). Untagged β_{2a} is coexpressed in lanes 2–5. (*C*) Titration of $_{CFP}[I–II]_{N\text{-intein}}$ to $_{C\text{-intein}}[III–IV]_{YFP}$ transfection ratio (plus CFP-β_{2a}). (*D*) Confocal images showing CFP, YFP, and QD fluorescence in cells coexpressing $_{CFP}[I–II]_{N\text{-intein}}$ + $_{C\text{-intein}}[III–IV]_{YFP}$ ± β_{2a}. (Scale bar, 10 μm.) (*E*) Flow cytometry dot plot of YFP and QD fluorescence. (*F*) Quantification of QD_{655} signal. *P = 0.0000427 compared with –β using two-tailed unpaired t test. n = 5, 50,000 cells per experiment.

for effective targeting to the cell surface (27, 28) (Fig. 2*F*). To selectively label surface channels, nonpermeabilized HEK293 cells coexpressing $_{CFP}[I–II]_{N\text{-intein}}$ + $_{C\text{-intein}}[III–IV]_{YFP}$ ± β_{2a} were sequentially labeled with biotinylated α-bungarotoxin (BTX) and streptavidin-conjugated fluorescent quantum dots (QD_{655}). Channel surface expression was analyzed by confocal imaging (Fig. 2*D*) and flow cytometry (Fig. 2*E*). Quantification of fluorescence intensity signals indicated $Ca_V\beta$ increased surface expression of intein-spliced α_{1C} eightfold, similar to the magnitude of response seen with WT α_{1C} (Fig. 2*F*).

We next compared functional characteristics of currents reconstituted with intein-spliced α_{1C} subunits to those obtained with their full-length WT counterparts. LTCCs reconstituted with WT α_{1C} + β_{2a} generated robust whole-cell currents (Fig. 3*A*) that activated at a threshold potential of –30 mV and peaked at 0 mV (Fig. 3*B*). Moreover, WT channels were strongly and rapidly inhibited by 1 μM nifedipine, with complete loss of current observed for 5 μM and 10 μM nifedipine (Fig. 3 *A–C*). Intein-spliced WT α_{1C} channels reconstituted with $_{CFP}[I–II]_{N\text{-intein}}$ + $_{C\text{-intein}}[III–IV]_{YFP}$ + β_{2a} displayed virtually identical whole-cell currents and similar sensitivity to nifedipine as WT α_{1C} + β_{2a} (Fig. 3 *D–F* and Table S1). By contrast, intein-spliced DHP-resistant α_{1C} channels displayed currents that were relatively insensitive to nifedipine (Fig. 3 *G–I*). Expressing either $_{CFP}[I–II]_{N\text{-intein}}$ or $_{C\text{-intein}}[III–IV]_{YFP}$ separately did not yield either ionic or gating currents in HEK293 cells (Fig. S2). This contrasts with previous reports that expressing the I–II domain of $Ca_V1.1$ (α_{1S}) in skeletal myotubes results in measurable gating charge (24, 25). The difference could be due to either the distinct Ca_V1 isoforms or cell types involved.

Expression and Trafficking of Intein-Spliced α_{1C} in Adult Cardiomyocytes. Having validated the split-intein strategy in HEK293 cells, we next used this method to express LTCCs in adult cardiomyocytes. We chose adenoviral vectors because they readily infect adult cardiac myocytes and have a relatively fast onset of protein expression (<24 h). This is important because adult cardiac myocytes begin to dedifferentiate after 3–4 d in culture (2). We were unable to generate adenoviruses incorporating full-length α_{1C}, a common finding for many investigators in the field, that is attributable to the large insert size of α_{1C} and regulatory elements (~7.2 kb) being at the packaging capacity limit of adenoviral vectors. By contrast, both intein-tagged α_{1C} moieties were readily packaged into adenoviral vectors (Fig. 4*A*). We infected adult rat cultured cardiomyocytes with $_{CFP}[I–II]_{N\text{-intein}}$ and either $_{C\text{-intein}}[III–IV]_{YFP}$ or $_{C\text{-intein}}[III–IV^{TQ/YM}]_{YFP}$ and examined cells for protein expression 48 h after infection. The cardiomyocyte infection was highly efficient, with >90% of cells exhibiting robust CFP/YFP fluorescence, confirming expression of the intein-flanked α_{1C} moieties (Fig. 4*B*). Western blotting confirmed that the split-intein–tagged α_{1C} moieties were spliced to generate full-length protein in adult cardiomyocytes. Whole-cell lysates probed with anti-α_{1C} antibody detected both endogenous and intein-spliced α_{1C} (Fig. 4*B*). Intein-spliced α_{1C} was readily distinguishable from endogenous α_{1C} due to the presence of fluorescent protein tags that endowed them with a higher molecular weight. Intein-spliced α_{1C} expression level was titratable, with increasing protein expression observed at higher adenoviral doses (Fig. 4*B*).

To determine whether intein-spliced α_{1C} expressed in cardiomyocytes trafficked to the cell surface, we sequentially exposed nonpermeabilized infected cardiomyocytes to biotinylated BTX and streptavidin-conjugated QD_{655}. Cardiomyocytes coexpressing $_{CFP}[I–II]_{N\text{-intein}}$ and $_{C\text{-intein}}[III–IV]_{YFP}$ displayed robust red QD_{655} fluorescence staining of the surface sarcolemma (Fig. 4*C* and Fig. S3). As a negative control, uninfected myocytes showed negligible QD fluorescence (Fig. 4*C* and Fig. S3). Similarly, cardiomyocytes expressing only $_{CFP}[I–II]_{N\text{-intein}}$ displayed minimal QD_{655} surface staining, indicating this moiety alone does not traffic to the cell surface (Fig. S3).

In adult ventricular myocytes, the close proximity of LTCCs and RyR2s at dyadic junctions can be demonstrated using immunofluorescence analyses showing a high degree of colocalization between endogenous α_{1C} and RyR2 (Fig. 4*D*), in agreement with previous reports (5). To determine whether intein-spliced α_{1C} was properly targeted to dyads we performed coimmunofluorescence experiments using anti-GFP and anti-RyR antibodies (Fig. 4*D*). Much of the anti-GFP staining was observed in regularly spaced transverse patterns that occurred with a periodicity of 1.8 μm, consistent with the staining pattern of t tubules in cardiomyocytes (Fig. 4*D*). Most importantly, quantitative analyses indicated intein-spliced α_{1C} colocalized with RyR2s to the same extent as endogenous channels, as demonstrated by similar Pearson's correlation coefficient values (Fig. 4*E*). Similar values were obtained by quantifying this colocalization independently using Li's intensity correlation coefficient (29) (Fig. S4).

Beyond localization at dyads, a subset of LTCCs in ventricular myocytes associate with caveolin-3 and target to caveolae (7, 30). Consistent with this, endogenous LTCCs exhibit significant colocalization with caveolin-3 in adult cardiomyocytes (Fig. S4). It is unknown whether α_{1C} subunits that are targeted to dyads are molecularly distinct from those associated with caveolin-3. One possible mechanism for differential LTCC targeting in cardiomyocytes could be alternative splicing of α_{1C}. We discovered that intein-spliced α_{1C} also colocalizes with endogenous caveolin-3 in cardiomyocytes (Fig. S4), indicating molecularly identical α_{1C} subunits can target to both dyads and caveolae.

Overall, these results show that intein-tagged α_{1C} halves expressed in cardiomyocytes are efficiently spliced together to generate an intact α_{1C} that traffics to dyads and associates with caveolin-3 similar to the endogenous protein. Because no $Ca_V\beta$ was coexpressed in these experiments, the results suggest intein-spliced α_{1C} associates with endogenous $Ca_V\beta$ to traffic to the cell surface.

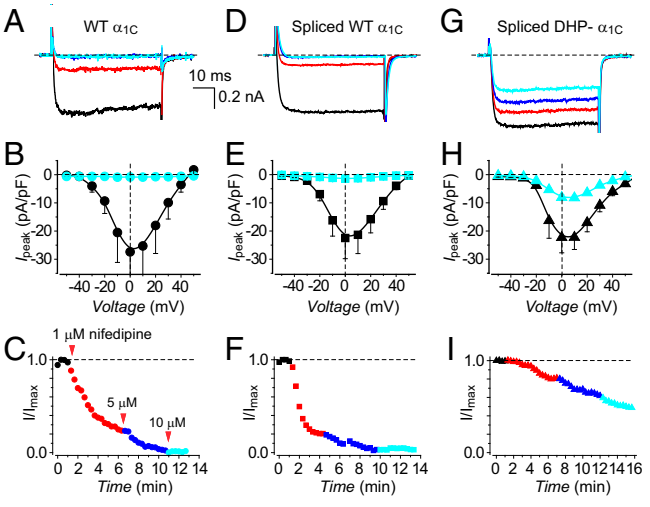

Fig. 3. Electrophysiological properties and DHP sensitivity of WT and split-intein–reconstituted LTCCs in HEK293 cells. (*A*) Exemplar Ba^{2+} currents from cells expressing full-length WT α_{1C} + β_{2a} in the absence (black trace) and presence of different nifedipine concentrations (1 μM, red; 5 μM, blue; 10 μM, cyan). (*B*) Population current-density versus voltage (*I–V*) relationship for cells expressing full-length WT α_{1C} + β_{2a} channels in the absence (black symbols) or presence (cyan symbols) of 10 μM nifedipine. $n = 7$ for each point. (*C*) Diary plots of nifedipine inhibition of full-length WT α_{1C} + β_{2a} channels. (*D–F*) Data for intein-spliced WT α_{1C} channels are in the same format as *A–C*. $n = 9$. (*G–I*) Data for intein-spliced DHP-resistant α_{1C} channels are in the same format as *A–C*. $n = 10$.

Functional Characterization of Intein-Spliced α_{1C} Subunits in Cardiomyocytes. We used whole-cell patch clamp to examine the functionality of intein-spliced α_{1C} subunits expressed in cardiomyocytes. Surprisingly, cardiomyocytes coexpressing $_{CFP}[I–II]_{N\text{-intein}}$ and either $_{C\text{-intein}}[III–IV]_{YFP}$ or $_{C\text{-intein}}[III–IV^{TQ/YM}]_{YFP}$ displayed only a marginal increase in Ba^{2+} current density compared with uninfected control myocytes (Fig. 5 *A–C*). One possible explanation for this result is that endogenous $Ca_V\beta$ subunits are rate-limiting for LTCC functional expression in heart. This interpretation would

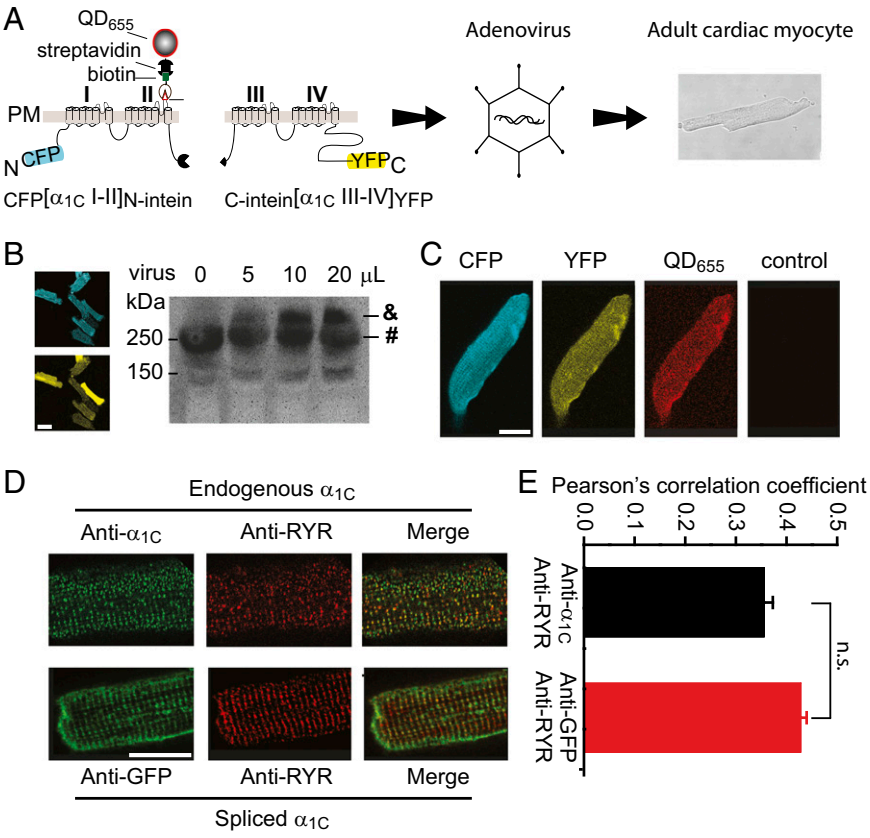

Fig. 4. Expression and subcellular targeting of intein-spliced α_{1C} in cardiac myocytes. (*A*) Schematic showing incorporation of split-intein–tagged α_{1C} moieties into adenovirus and infection of cardiomyocytes. (*B*, *Left*) Confocal images showing high efficiency expression of CFP- and YFP-tagged split-intein α_{1C} moieties in adult cardiomyocytes. (Scale bar, 50 μm.) (*B*, *Right*) Western blot (anti-α_{1C} antibody) detection of endogenous (#) and intein-spliced (&) α_{1C} subunits. (*C*) Confocal images of CFP, YFP, and QD_{655} fluorescence in a cardiomyocyte expressing intein-spliced α_{1C}. Control shows absence of QD_{655} staining in an uninfected cell. (Scale bar, 20 μm.) (*D*, *Upper*) Immunostaining of endogenous α_{1C} (anti-α_{1C}, green) and RyR (anti-RyR, red) in an uninfected cardiomyocyte. (*D*, *Lower*) Immunostaining of intein-spliced α_{1C} (anti-GFP, green) and endogenous RYR (anti-RyR, red). (Scale bar, 20 μm.) (*E*) Colocalization analyses.

be consistent with prior observations that overexpressing $Ca_V\beta$s alone in heart causes a several-fold increase in LTCC current density (11, 31). An alternate possibility was that the intein-spliced α_{1C} subunits were not functional despite making it to the cell surface (Fig. 4). To distinguish between the two possibilities we recorded currents in cardiomyocytes expressing either intein-spliced WT or DHP-resistant α_{1C} in the presence of 10 μM nifedipine (Fig. 5*D*). Under these conditions, cardiomyocytes expressing intein-spliced DHP– α_{1C} subunits expressed currents that were on average threefold larger than those expressing spliced WT α_{1C}, demonstrating that the expressed channels are functional (Fig. 5 *D* and *E*). We obtained a similarly large DHP-resistant current in cardiomyocytes coinfected with $_{CFP}$[I–II]$_{N\text{-intein}}$ and $_{C\text{-intein}}$[III–IV$^{TO/YM}$] expressed in a bicistronic adenovirus vector (Fig. S5). The bicistronic strategy can be used to overcome potential concerns that directly fusing fluorescent proteins to the α_{1C} fragments could disrupt aspects of their functions in some unanticipated way. Because DHP block of $Ca_V1.2$ is known to be voltage- and state-dependent, we examined whether we could achieve greater nifedipine separation of WT and DHP-resistant α_{1C} by using a –50 mV holding potential and 2 mM Ca^{2+} as charge carrier (Fig. S6). Under these conditions, WT $Ca_V1.2$ currents elicited by a ramp protocol were deeply inhibited by 10 μM nifedipine, whereas myocytes expressing intein-spliced DHP-resistant α_{1C} displayed a sevenfold larger remnant current (Fig. S6).

To determine the functional competence of intein-spliced α_{1C} to trigger CICR at dyads, we measured rhod-2–reported Ca^{2+} transients using line scan confocal microscopy (Fig. 6). Control uninfected cells responded to 1 Hz field stimulation with robust basal Ca^{2+} transients that were inhibited by 1 μM nifedipine (Fig. 6 *A* and *D*). In myocytes expressing either intein-spliced WT (Fig. 6*B*) or DHP– (Fig. 6*C*) α_{1C}, basal Ca^{2+} transients were marginally larger than observed in uninfected controls, consistent with a modest increase in the number of surface LTCCs (Fig. 6*D*). Ca^{2+} transients in cardiomyocytes expressing intein-spliced WT α_{1C} were inhibited by 1 μM nifedipine (90% inhibition), with most cells unresponsive to field stimulation (Fig. 6 *B* and *D*). By contrast, cardiomyocytes expressing spliced DHP-resistant α_{1C} were only modestly inhibited by 1 μM nifedipine (20% inhibition) and virtually all cells remained responsive to field stimulation. Exposure of cardiomyocytes expressing spliced WT α_{1C} to 5 μM nifedipine completely eliminated Ca^{2+} transients in response to field stimulation in eight out of eight cells (Fig. 6*E*), whereas six out of nine cells expressing spliced DHP-resistant α_{1C} remained responsive at this higher DHP concentration (Fig. 6*F*).

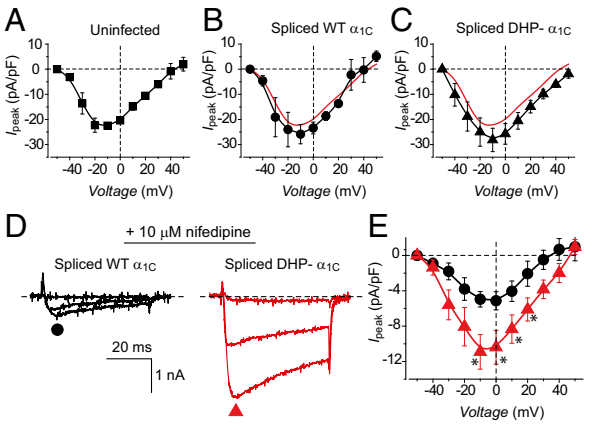

Fig. 5. Electrophysiological characterization of intein-spliced WT and DHP-resistant α_{1C} in cardiac myocytes. Population *J*–*V* relationships in (*A*) uninfected cardiomyocytes (control), (*B*) myocytes expressing intein-spliced WT α_{1C}, or (*C*) intein-spliced DHP– α_{1C}. (*D* and *E*) Exemplar current traces and population *J*–*V* curves from cardiomyocytes expressing either intein-spliced WT α_{1C} (black trace and symbols, $n = 9$) or DHP– α_{1C} (red trace and symbols, $n = 8$) channels in the presence of 10 μM nifedipine. $^*P = 0.018$ (–10 mV), $^*P = 0.0324$ (0 mV), $^*P = 0.048$ (10 mV), and $^*P = 0.04$ (20 mV) using two-tailed unpaired *t* test.

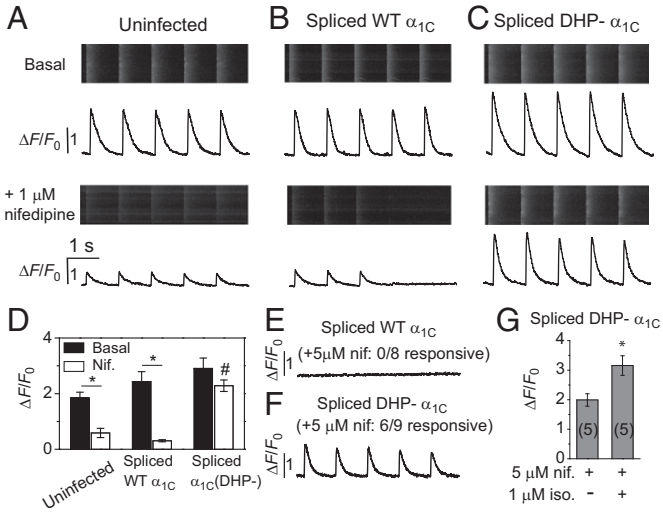

Fig. 6. Participation of intein-spliced WT and DHP– α_{1C} in CICR in cardiomyocytes. (*A*, *Upper*) The rhod-2-reported Ca^{2+} transients in an uninfected (UT) cardiomyocyte paced with 1 Hz field stimulation. (*A*, *Lower*) Ca^{2+} transients from UT myocyte in the presence of 1 μM nifedipine. (*B* and *C*) Ca^{2+} transients from cardiomyocytes expressing intein-spliced WT (α_{1C}) and DHP– α_{1C}, respectively. Same format as *A*. (*D*) Impact of 1 μM nifedipine on Ca^{2+} transient amplitudes. * $P = 0.0014$ (UT), * $P = 0.0003$ (α_{1C}), two-tailed unpaired *t* test. #, significantly different from control and intein-spliced WT α_{1C} +nifedipine using one-way ANOVA [$F(2, 12) = 47.48$, $P = 2E\text{-}6$] and Bonferroni pairwise comparisons, $n = 5$ cells. (*E*) CICR is abolished by 5 μM nifedipine in cardiomyocytes expressing intein-spliced WT α_{1C}. (*F*) Persistence of CICR in cardiomyocytes expressing intein-spliced DHP– α_{1C} in 5 μM nifedipine. (*G*) A total of 1 μM isoproterenol potentiates Ca^{2+} transients triggered by intein-spliced DHP– α_{1C}, *$P = 0.018$.

With the ability to completely isolate intein-spliced DHP-resistant α_{1C}-stimulated Ca^{2+} transients with 5 μM nifedipine, we examined whether this channel was permissive for sympathetic up-regulation of EC coupling under these experimental conditions. Exposure of cardiomyocytes expressing spliced DHP-resistant α_{1C} to 5 μM nifedipine + 1 μM isoproterenol resulted in Ca^{2+} transients with an elevated peak compared with those obtained with 5 μM nifedipine alone (Fig. 6*G*). The sympathetic elevation of Ca^{2+} transients under these conditions is likely due to a combination of PKA-dependent phosphorylation of $Ca_V1.2$, RYR2, and phospholamban (32).

Discussion

We have developed a unique method to readily manipulate tagged α_{1C} expression in isolated adult cardiomyocytes. The unique technology offers clear advantages over using heterologous expression systems to study the functional properties of cardiac LTCCs. Heterologous cells lack the unique cytoarchitecture of adult cardiomyocytes. Consequently, questions such as the mechanisms underlying differential LTCC targeting to dyads and caveolae, or their putative role in pathological cardiac hypertrophy, cannot be studied in noncardiomyocytes. It has also proven difficult to determine the mechanism of PKA-induced enhancement of LTCCs from heterologous expression experiments. Based on studies in HEK293 cells, it was suggested that phosphorylation of Ser1928 in α_{1C} and Ser478/Ser479 in β_{2a} was critical for PKA regulation of LTCCs (33, 34). However, the putative role of these phosphorylation sites in PKA regulation of LTCC was ruled out using α_{1C}[Ser1928Ala] mutant channels and truncated-β_2 knock-in mice (35, 36), as well as experiments in isolated adult cardiomyocytes (11, 37). More recent data using HEK293 point to an essential role for phosphorylation of Ser1700 and Thr1704 in PKA regulation of LTCCs (38). The importance of these residues has not been directly confirmed in cardiac myocytes. Overall, these discrepancies emphasize the importance of addressing questions pertaining to LTCC trafficking and functional regulation in the context of actual heart cells. A caveat is that the isoproterenol-induced increase in peak evoked Ca^{2+} release we measured was relatively modest and likely also includes contributions by PKA regulation of RYR and phospholamban. In part, the relatively modest response may be attributable to the use of rat cardiomyocytes in which PKA modulation of $Ca_V1.2$ is much less robust than in other species such as guinea pig (11). We are currently working to establish conditions for strong PKA modulation of spliced DHP-insensitive α_{1C} in guinea pig cardiomyocytes.

Knock-in mouse models are the gold standard for defining structure–function mechanisms of proteins in heart. The approach of manipulating α_{1C} expression with adenoviral vectors in isolated adult cardiomyocytes offers several advantages over knock-in mouse models. First, knock-in mice are costly and take up to 2 y to generate, making their routine use for in-depth structure–function studies requiring many different constructs impractical. By comparison, split-intein adenoviruses are more cost and time effective. Second, certain questions cannot be pursued in knock-in mice due to lethality of the knocked in gene. For example, knock-in mice featuring C-terminal truncations of α_{1C} unexpectedly display a marked decrease in L-type calcium current and die shortly after birth due to heart failure (39, 40). This precludes the use of knock-in mice to pursue relevant questions regarding the role of α_{1C} C terminus in LTCC trafficking and functional regulation in adult cardiomyocytes. Third, the adenoviral infection approach permits questions to be easily addressed in different species. This is important because the functional properties of murine cardiomyocytes differ in several critical ways from those of human, such as the action potential duration being considerably shorter in mice (41). There have been scattered reports of successful expression of LTCC α_{1C} subunits in adult cardiomyocytes (37, 42, 43). Previously, by additionally deleting the fiber gene from the standard adenoviral vector backbone (E1 and E3 deleted) and generating a complementing stable cell line, we were able to generate adenovirus containing full-length α_{1C} (37, 42). However, this system proved unstable and further attempts to generate new adenoviruses were unsuccessful. There has been one report using lentivirus to express α_{1C} subunits in adult rat cardiomyocytes (44). We generated lentiviruses expressing GFP-tagged α_{1C} truncated in the C terminus at residue 1905, which transduced HEK293 cells efficiently, expressing α_{1C}[1905]–GFP within 48 h. However, in our hands, the transduction efficiency of adult cardiomyocytes was low, and required several days for transgene expression, a problematic feature given the short half-life of rod-shaped cardiomyocytes in culture. Recently, a biolistic transfection method was adapted to express α_{1C} in adult rat ventricular myocytes (41). Compared with our approach, the biolistic method suffers from high toxicity (~10% viable cells) and relatively low transfection efficiency (~30% of surviving cells express transgene) (45).

Our unique application of split-intein technology engineers functional expression of a large protein with high efficiency in adult heart cells. Beyond LTCCs there are many other large cardiac proteins (e.g., voltage-gated sodium channel, ankyrin, spectrin, myosin, ryanodine receptor, and titin) whose structure–function properties, trafficking, and functional modulation in heart are of major interest, but currently only accessible using knock-in mice. The split-intein approach can be extended to explore the functional properties of many other large proteins in cardiomyocytes. Overall, the split-intein method expands the toolkit available, which includes high-capacity HSV-1 amplicon vectors (46), for manipulating expression of large genes in primary cardiac myocytes.

Materials and Methods

Generation of Plasmid and Adenoviral Vectors. GenBank IDs of cDNAs used are provided in Table S2. Detailed cloning strategies to generate expression plasmids are provided in *SI Materials and Methods*. PCR primer sequences used for cloning are provided in Table S3. Replication-deficient adenoviruses

were generated using the Clontech Adeno-X System 3. Viral expansion and purification was carried out as described (31).

Cell Culture and Transfection/Infection. HEK293 cells cultured on 60 mm dishes were transfected with the appropriate cDNA (6 μg each) and T-antigen (1 μg) using calcium phosphate precipitation. Adult rat cardiomyocytes were prepared as described (31, 47) and cultured in medium supplemented with 0.5 μM cytochalasin D to preserve cell morphology (48). Cells were infected with 5–15 μL of viral stock in a final volume of 1–2 mL.

Quantum Dot Detection of Cell Surface BBS-Tagged LTCCs. Surface LTCCs in HEK293 cells or cardiomyocytes were labeled with quantum-dots as described (21), and assayed by flow cytometry using a BD LSR II Cell Analyzer (BD Biosciences). Flow cytometry data were analyzed using FloJo Software (21).

Intracellular Calcium Transient Measurements. Primary myocytes in culture were loaded with the calcium-sensing dye rhod2–AM. Evoked intracellular calcium transients were measured as described in *SI Materials and Methods*.

Image Processing and Analysis. Confocal images were analyzed using ImageJ software and background subtracted. Colocalization of CFP/YFP, α_{1C}/RyR, and α_{1C}/caveolin-3 was carried out using the ImageJ JaCoP plugin. Colocalization in two channels was quantified using Pearson's and Li's colocalization coefficient algorithms in JaCoP (29).

Electrophysiology. Whole-cell recordings were conducted on HEK293 cells 48 h posttransfection using an EPC-8 patch clamp amplifier (HEKA Electronics) controlled by PULSE software as previously described (21, 28). Whole-cell recordings of rat ventricular myocytes were performed as described previously (31).

Analysis and Statistics. Data were plotted and statistical analyses performed in Origin software using built-in functions. Significant differences between means ($P < 0.05$, $P < 0.01$) were determined using Student *t* test for comparison between two groups, or one-way ANOVA followed by Bonferroni post hoc analyses for comparisons involving more than two groups. Data are represented as means ± SEM.

ACKNOWLEDGMENTS. We thank Prof. Tom W. Muir (Princeton University) for the generous gift of the plasmids containing *N. punctiforme* DnaE split-intein cDNA and Ming Chen for technical support. This work was supported by Grant R01 HL 069911 from the National Institutes of Health (to H.M.C.). H.M.C. is an Established Investigator of the American Heart Association.

1. Bers D (2001) *Excitation-Contraction Coupling and Cardiac Contractile Force* (Kluwer Academic Publishers, Dordrecht, the Netherlands), 2nd Ed, p 427.
2. Louch WE, Sheehan KA, Wolska BM (2011) Methods in cardiomyocyte isolation, culture, and gene transfer. *J Mol Cell Cardiol* 51(3):288–298.
3. Vinge LE, Raake PW, Koch WJ (2008) Gene therapy in heart failure. *Circ Res* 102(12): 1458–1470.
4. Bers DM (2002) Cardiac excitation-contraction coupling. *Nature* 415(6868):198–205.
5. Scriven DR, Dan P, Moore ED (2000) Distribution of proteins implicated in excitation-contraction coupling in rat ventricular myocytes. *Biophys J* 79(5):2682–2691.
6. Fabiato A (1983) Calcium-induced release of calcium from the cardiac sarcoplasmic reticulum. *Am J Physiol* 245(1):C1–C14.
7. Balijepalli RC, Foell JD, Hall DD, Hell JW, Kamp TJ (2006) Localization of cardiac L-type Ca(2+) channels to a caveolar macromolecular signaling complex is required for beta (2)-adrenergic regulation. *Proc Natl Acad Sci USA* 103(19):7500–7505.
8. Makarewich CA, et al. (2012) A caveolae-targeted L-type Ca^{2}+ channel antagonist inhibits hypertrophic signaling without reducing cardiac contractility. *Circ Res* 110(5): 669–674.
9. Shaw RM, Colecraft HM (2013) L-type calcium channel targeting and local signalling in cardiac myocytes. *Cardiovasc Res* 98(2):177–186.
10. Reuter H, Scholz H (1977) The regulation of the calcium conductance of cardiac muscle by adrenaline. *J Physiol* 264(1):49–62.
11. Miriyala J, Nguyen T, Yue DT, Colecraft HM (2008) Role of CaVbeta subunits, and lack of functional reserve, in protein kinase A modulation of cardiac CaV1.2 channels. *Circ Res* 102(7):e54–e64.
12. Zong X, et al. (1995) On the regulation of the expressed L-type calcium channel by cAMP-dependent phosphorylation. *Pflugers Arch* 430(3):340–347.
13. Catterall WA (2010) Signaling complexes of voltage-gated sodium and calcium channels. *Neurosci Lett* 486(2):107–116.
14. Perler FB, et al. (1994) Protein splicing elements: Inteins and exteins—a definition of terms and recommended nomenclature. *Nucleic Acids Res* 22(7):1125–1127.
15. Lockless SW, Muir TW (2009) Traceless protein splicing utilizing evolved split inteins. *Proc Natl Acad Sci USA* 106(27):10999–11004.
16. Muralidharan V, Muir TW (2006) Protein ligation: An enabling technology for the biophysical analysis of proteins. *Nat Methods* 3(6):429–438.
17. Iwai H, Züger S, Jin J, Tam PH (2006) Highly efficient protein trans-splicing by a naturally split DnaE intein from Nostoc punctiforme. *FEBS Lett* 580(7):1853–1858.
18. Zettler J, Schütz V, Mootz HD (2009) The naturally split Npu DnaE intein exhibits an extraordinarily high rate in the protein trans-splicing reaction. *FEBS Lett* 583(5): 909–914.
19. Catterall WA (2000) Structure and regulation of voltage-gated Ca2+ channels. *Annu Rev Cell Dev Biol* 16:521–555.
20. Sekine-Aizawa Y, Huganir RL (2004) Imaging of receptor trafficking by using alpha-bungarotoxin-binding-site-tagged receptors. *Proc Natl Acad Sci USA* 101(49):17114–17119.
21. Yang T, Xu X, Kernan T, Wu V, Colecraft HM (2010) Rem, a member of the RGK GTPases, inhibits recombinant CaV1.2 channels using multiple mechanisms that require distinct conformations of the GTPase. *J Physiol* 588(Pt 10):1665–1681.
22. He M, Bodi I, Mikala G, Schwartz A (1997) Motif III S5 of L-type calcium channels is involved in the dihydropyridine binding site. A combined radioligand binding and electrophysiological study. *J Biol Chem* 272(5):2629–2633.
23. Mitterdorfer J, et al. (1996) Two amino acid residues in the IIIS5 segment of L-type calcium channels differentially contribute to 1,4-dihydropyridine sensitivity. *J Biol Chem* 271(48):30330–30335.
24. Ahern CA, et al. (2001) Intramembrane charge movements and excitation- contraction coupling expressed by two-domain fragments of the Ca2+ channel. *Proc Natl Acad Sci USA* 98(12):6935–6940.
25. Flucher BE, Weiss RG, Grabner M (2002) Cooperation of two-domain Ca(2+) channel fragments in triad targeting and restoration of excitation-contraction coupling in skeletal muscle. *Proc Natl Acad Sci USA* 99(15):10167–10172.
26. Raghib A, et al. (2001) Dominant-negative synthesis suppression of voltage-gated calcium channel Cav2.2 induced by truncated constructs. *J Neurosci* 21(21):8495–8504.
27. Buraei Z, Yang J (2010) The ß subunit of voltage-gated Ca2+ channels. *Physiol Rev* 90(4):1461–1506.
28. Fang K, Colecraft HM (2011) Mechanism of auxiliary β-subunit-mediated membrane targeting of L-type (Ca(V)1.2) channels. *J Physiol* 589(Pt 18):4437–4455.
29. Bolte S, Cordelières FP (2006) A guided tour into subcellular colocalization analysis in light microscopy. *J Microsc* 224(Pt 3):213–232.
30. Nichols CB, et al. (2010) Sympathetic stimulation of adult cardiomyocytes requires association of AKAP5 with a subpopulation of L-type calcium channels. *Circ Res* 107(6):747–756.
31. Colecraft HM, et al. (2002) Novel functional properties of Ca(2+) channel beta subunits revealed by their expression in adult rat heart cells. *J Physiol* 541(Pt 2):435–452.
32. Luo W, et al. (1998) Transgenic approaches to define the functional role of dual site phospholamban phosphorylation. *J Biol Chem* 273(8):4734–4739.
33. Bünemann M, Gerhardstein BL, Gao T, Hosey MM (1999) Functional regulation of L-type calcium channels via protein kinase A-mediated phosphorylation of the beta(2) subunit. *J Biol Chem* 274(48):33851–33854.
34. Gao T, et al. (1997) cAMP-dependent regulation of cardiac L-type Ca2+ channels requires membrane targeting of PKA and phosphorylation of channel subunits. *Neuron* 19(1):185–196.
35. Brandmayr J, et al. (2012) Deletion of the C-terminal phosphorylation sites in the cardiac β-subunit does not affect the basic β-adrenergic response of the heart and the Ca(v)1.2 channel. *J Biol Chem* 287(27):22584–22592.
36. Lemke T, et al. (2008) Unchanged beta-adrenergic stimulation of cardiac L-type calcium channels in Ca v 1.2 phosphorylation site S1928A mutant mice. *J Biol Chem* 283(50):34738–34744.
37. Ganesan AN, Maack C, Johns DC, Sidor A, O'Rourke B (2006) Beta-adrenergic stimulation of L-type Ca2+ channels in cardiac myocytes requires the distal carboxyl terminus of alpha1C but not serine 1928. *Circ Res* 98(2):e11–e18.
38. Fuller MD, Emrick MA, Sadilek M, Scheuer T, Catterall WA (2010) Molecular mechanism of calcium channel regulation in the fight-or-flight response. *Sci Signal* 3(141):ra70.
39. Fu Y, et al. (2011) Deletion of the distal C terminus of CaV1.2 channels leads to loss of beta-adrenergic regulation and heart failure in vivo. *J Biol Chem* 286(14):12617–12626.
40. Domes K, et al. (2011) Truncation of murine CaV1.2 at Asp-1904 results in heart failure after birth. *J Biol Chem* 286(39):33863–33871.
41. Nerbonne JM, Kass RS (2005) Molecular physiology of cardiac repolarization. *Physiol Rev* 85(4):1205–1253.
42. Ganesan AN, et al. (2005) Reverse engineering the L-type Ca2+ channel alpha1c subunit in adult cardiac myocytes using novel adenoviral vectors. *Biochem Biophys Res Commun* 329(2):749–754.
43. Walsh KB, Zhang J, Fuseler JW, Hilliard N, Hockerman GH (2007) Adenoviral-mediated expression of dihydropyridine-insensitive L-type calcium channels in cardiac ventricular myocytes and fibroblasts. *Eur J Pharmacol* 565(1-3):7–16.
44. Thiel WH, et al. (2008) Proarrhythmic defects in Timothy syndrome require calmodulin kinase II. *Circulation* 118(22):2225–2234.
45. Dou Y, et al. (2010) Normal targeting of a tagged Kv1.5 channel acutely transfected into fresh adult cardiac myocytes by a biolistic method. *Am J Physiol Cell Physiol* 298(6):C1343–C1352.
46. Ferrera R, et al. (2005) Efficient and non-toxic gene transfer to cardiomyocytes using novel generation amplicon vectors derived from HSV-1. *J Mol Cell Cardiol* 38(1): 219–223.
47. Xu X, Colecraft HM (2009) Primary culture of adult rat heart myocytes. *J Vis Exp*, 10.3791/1308.
48. Tian Q, et al. (2012) Functional and morphological preservation of adult ventricular myocytes in culture by sub-micromolar cytochalasin D supplement. *J Mol Cell Cardiol* 52(1):113–124.